Quantum Chemical Study of Trimolecular Reaction Mechanism between Nitric Oxide and Oxygen in the Gas Phase

ARTICLE *in* THE JOURNAL OF PHYSICAL CHEMISTRY A · JULY 2009

Impact Factor: 2.69 · DOI: 10.1021/jp900484s · Source: PubMed

4 AUTHORS, INCLUDING:

Oleg B. Gadzhiev
Nizhny Novgorod State University
14 PUBLICATIONS **66** CITATIONS
SEE PROFILE

Stanislav K. Ignatov
N.I. Lobachevsky State University of Nizhn…
69 PUBLICATIONS **585** CITATIONS
SEE PROFILE

Artem E. Masunov
University of Central Florida
147 PUBLICATIONS **2,510** CITATIONS
SEE PROFILE

Quantum Chemical Study of Trimolecular Reaction Mechanism between Nitric Oxide and Oxygen in the Gas Phase

Oleg B. Gadzhiev,*,† Stanislav K. Ignatov,† Alexei G. Razuvaev,† and Artëm E. Masunov*,‡

Department of Chemistry, N.I. Lobachevsky State University of Nizhny Novgorod, 23 Gagarin Avenue, Nizhny Novgorod 603950, Russia, and NanoScience Technology Center, Department of Chemistry, and Department of Physics, University of Central Florida, 12424 Research Parkway, Suite 400, Orlando, Florida 32826

Received: January 16, 2009; Revised Manuscript Received: May 8, 2009

Singlet and triplet potential energy surfaces of the reaction between molecular oxygen and two nitric oxide(II) molecules were studied by quantum chemical methods (coupled cluster, CASSCF, and density functional theory: B3LYP, TPSS, VSXC, BP86, PBE, B2-PLYP, B2K-PLYP). Elementary steps involving various N_2O_4 isomers (cyclic, *cis*−*cis*-, *cis*−*trans*-, *trans*−*trans*-ONOONO, *cis*- and *trans*-$ONONO_2$, O_2NNO_2) were considered, as well as weakly bound molecular clusters preceding formation of O_2NNO_2, and Coupe-type quasi-aromatic hexagonal ring intermediate $NO_2 \cdot O_2N$. We found that activation energy strongly depends on the conformation of ONOONO peroxide, which is formed barrierlessly. The best agreements with experimental values were achieved by the B3LYP functional with aug-pc3 basis set. The lowest transition state (TS) energies correspond to the following reaction channel: $2NO + O_2$ (0 kJ/mol) → *cis*−*cis*-ONOONO (−45 kJ/mol) → TS1 → $NO_2 \cdot O_2N$ (−90 kJ/mol) → TS2 → *cis*-$ONONO_2$ (−133 kJ/mol)→ TS3 → *trans*-$ONONO_2$ (−144 kJ/mol) → TS4 → O_2NNO_2 (−193 kJ/mol). A valley ridge inflection (VRI) point is located on the minimum energy path (MEP) connecting $NO_2 \cdot O_2N$ and *cis*-$ONONO_2$. The energy landscape between $NO_2 \cdot O_2N$ and CC-TS2 can be classified as a downhill valley-pitchfork VRI bifurcation according to a recent classification of bifurcation events [Quapp, W. *J. Mol. Struct.* **2004**, *95*, 695−696]. The first and second transition states correspond to barrier heights of 10.6 and 37.0 kJ/mol, respectively. These values lead to the negative temperature dependence of the rate constant. The apparent activation enthalpy of the overall reaction was calculated to be $\Delta_r H^{\ddagger}(0) = -4.5$ kJ/mol, in perfect agreement with the experimental value.

1. Introduction

For more than 75 years of study,[1−3] the nitric oxide(II) oxidation in the gas phase

$$2NO + O_2 \rightarrow 2NO_2 \quad (1)$$

has been a classic example of an elementary trimolecular reaction.[1,4] It became a part of many textbooks and monographs on chemical kinetics and physical chemistry. Nonetheless, its mechanism still remains a matter of debate.[5−10] It was established[6] that at a temperature range between 273 and 600 K the reaction has the third kinetic order with negative apparent activation energy, which becomes positive above 650 K. Various rate constants had been reported,[5−10] of which the expression[6] $k = 1.2 \times 10^3 e^{530/T}$ L^2 mol^{-2} s^{-1} seems to be the most reliable.

On the basis of experimental measurements, several kinetic models have been suggested to describe the reaction mechanism and to explain the negative temperature dependence of the rate constant:

(1) The first is the synchronous trimolecular reaction $2NO + O_2 \rightarrow [ONOONO]^{\ddagger} \rightarrow 2NO_2$.[1]

(2) The second is the two-step mechanism including NO dimer formation:[5,7,8,10,11]

$$NO + NO \rightarrow (NO)_2$$

$$(NO)_2 + O_2 \rightarrow 2NO_2$$

(3) The third is the two-step mechanism including NO_3 formation:[9,12−15]

$$NO + O_2 \rightarrow NO_3$$

$$NO + NO_3 \rightarrow 2NO_2$$

Inaccuracy in the experimental data due to a wide variation of conditions and corresponding differences in experimental mechanisms does not allow one to choose between the mechanisms conclusively.[16] Quantum chemical calculations of the intermediates and transition states (TS), predicted by the proposed mechanisms (1−3), lead to high activation energies.[16−20] On the basis of this fact, some authors suggested that the reaction mechanism is different from (1)−(3).[17−20]

One of the alternative mechanisms was proposed by McKee,[21] who considered the peroxide ONOONO as a key intermediate (not the transition state, like in mechanism 1). Indeed, the activation enthalpy of the reaction $2NO + O_2 \rightarrow$ ONOONO is negative at the QCISD(T)/6-31+G(2df)//MP2/6-31G(d)+DFT/ZPC theory level. Later studies[22,23] at the levels MP2/6-311G(d), B3LYP/cc-pVDZ, and B3P86/cc-pVDZ established that ONOONO may exist in different conformers (Scheme 1): *s-cis*−*cis* (**CC**),

* Corresponding authors. These authors contributed equally to this work. E-mail: euriscomail@mail.ru (O.B.G.); amasunov@mail.ucf.edu (A.E.M.).
† N.I. Lobachevsky State University of Nizhny Novgorod.
‡ University of Central Florida.

10.1021/jp900484s CCC: $40.75
Published on Web 07/17/2009

SCHEME 1: Three Conformers of the ONOONO Peroxide: (a) *s-cis−cis* (CC), (b) *s-trans−trans* (TT), (c) *s-cis−trans* (CT), and (d) Planar Cyclic (CC-INT)

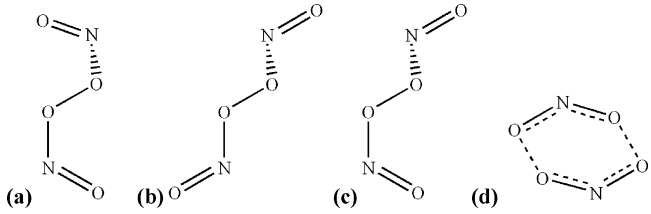

cyclic (**CC-INT**), *s-cis−trans* (**CT**), and *s-trans−trans* (**TT**). The latter structure is the intermediate, studied by McKee.[21]

When the three conformers mentioned above are introduced[24] into the mechanism suggested by McKee,[21] the potential energy surface (PES) becomes more complicated, as shown by Olson et al.[24] They found three reaction channels involving previously[22,23] reported ONOONO conformers as well as interconversion reactions between the conformers. All energies determined by Olson et al.[24] at the B3LYP/6-311G(d) level are collected in Figure 1 in parentheses. Structures of the same name are similar if additional comments are not presented. First (and main) reaction path includes rearrangement of **CC** via **CC-TS1** with low-energy barrier to intermediate **CC-INT**, which isomerizes to *s-cis*-$ONONO_2$ via **CC-TS2**. However, Olson et al.[24] did not investigate the rest of the reaction pathway, leading to the product of reaction 1. They also built the second path up to **CT-INT**, while **CT-TS2** was reported to be a second-order saddle point. Thus, the proposed[24] pathway to *s-trans*-$ONONO_2$ was not built unambiguously. The third path, originally proposed by McKee[21] for the **TT** intermediate, was changed from O−O-bond cleavage with forming of two NO_2 to isomerization to O_2NNO_2.

Despite the progress in understanding the potential surface topology,[24] analysis of the complete reaction pathway was never attempted, and the existence of the high activation barriers in unexplored areas cannot be ruled out with confidence. Besides, only the singlet PES of reaction 1 was studied in the previous works. There is a possibility for the reaction on the triplet PES to proceed through other intermediates with lower activation energy. It is also necessary to note that the use of only one density functional theory (DFT) level using B3LYP exchange-correlation functional combined with modest basis sets (no diffuse functions) for geometry optimization does not ensure confidence in the interaction energy values for weakly bound complexes.

The recent attempt to refine the PES with a higher theory level (G2M(CC)//G96LYP/6-31+G*) was made by Choi and Lin.[25] However, they did not describe TS geometry, which made it difficult to evaluate the accuracy of their values.

The present work is aimed to build a complete PES of the $2NO + O_2$ reactive system in both singlet and triplet multiplicities. We use the larger basis sets and different exchange-correlation functionals to test McKee's[21] and Olson's[24] mechanism. In addition to DFT, the systems are studied with high-level ab initio wave function theories, including geometry optimizations by Coupled Cluster Singles and Doubles (CCSD) and Complete Active Space Self Consistent Field (CASSCF) methods and single point energy calculations by CCSD(T) method.

2. Computational Details

The Gaussian 03 suite of computer programs[26] was used for most of the reported calculations excluding optimizations at the levels RI-B2PLYP[27] and B2K-PLYP.[28] The two last implemented in the ORCA suite of computer programs[29] was used for geometry optimization at the levels RI-B2PLYP[27,30,31] and B2K-PLYP.[28,32,33] Moltran[34] and GaussView03[35] were used for visualization and analysis of the results.

Density functional theory with different types of exchange-correlation functionals was used: hybrid GGA (B3LYP), non-empirical meta-GGA (TPSS), empirical meta-GGA (VSXC), nonempirical GGA (PBE), empirical GGA (BP86), double hybrid RI-B2PLYP, and double hybrid B2K-PLYP with semiempirical van-der-Waals correction.[27] These functions have the least mean absolute deviation from thermodynamic values collected in databases G2/97, G3/99, and G3/05 among functionals of the present types.[36] Calculations were made with four different types of the basis sets: 6-311G(d), aug-cc-pVDZ, and *aug-pc-3*. The latter basis set belongs to the *pc-n/aug-pc-n*[37−42] group, developed especially for use with DFT. The properties of nitrogen oxides[39] were included in the training set during its parameter fitting process. For selected intermediates on the singlet PES, we also performed geometry optimization using CCSD and CASSCF (with active space varied up to (26,16)) methods with the 6-311G(d) basis set and single point energy calculations by the CCSD(T) method.

We paid special attention to the spin contamination in the systems studied, as indicated by the deviation of the mean value of the spin operator $\langle \hat{S}^2 \rangle$ from its ideal value for a pure spin state. The contribution of the higher spin states for singlet particles was found to be extremely small. In doublet and triplet states, spin contamination did not exceed 0.004 au. Stability check of the SCF solution was performed for all of the stationary points.

To avoid false convergence due to small gradients on a flat PES, tight convergence criteria were used in the SCF procedure and geometry optimization, with the exception of two difficult cases (CC-TS3 and TS-O_2NNO_2-i-*trans*-$ONONO_2$), where the convergence tolerance was reduced to 1 millihartree. Keyword Grid=UltraFine was used for some of the key structures to reduce numerical integration errors while solving the Kohn−Sham equations. Because we found small influence of the integration grid on relative energies, the geometries and vibrational frequencies were calculated with Grid=FineGrid keyword (the default).

Harmonic vibrational frequency analysis was completed for all stationary points to ensure their correct assignment as to local minima (all vibrational frequencies are positive) or transition states (single imaginary frequency). In addition, all transition states were verified by Intrinsic Reaction Coordinate method (IRC). Continuous reaction paths on the singlet PES (Figure 1) were established between all found stationary points by means of IRC calculations. To avoid errors in the PES topology analysis for the most complicated cases, search for a local minimum was conducted from both the initial point and the TS found initially.

3. Results and Discussion

3.1. General Remarks. All intermediates on the singlet PES optimized at B3LYP/6-311+G(2d), B3LYP/aug-pc3, and TPSS/6-311+G(2d) theory levels confirmed the ones reported by Olson et al.[24] Other theory levels found some of the intermediates to be unstable. This instability, however, did not involve the main reaction channel. In agreement with ref 24, the main reaction channel involves the hexagonal cyclic intermediate **CC-INT** (see Figure 1). Total energies of the optimized structures are reported in Table 1, and interatomic distances in the fully

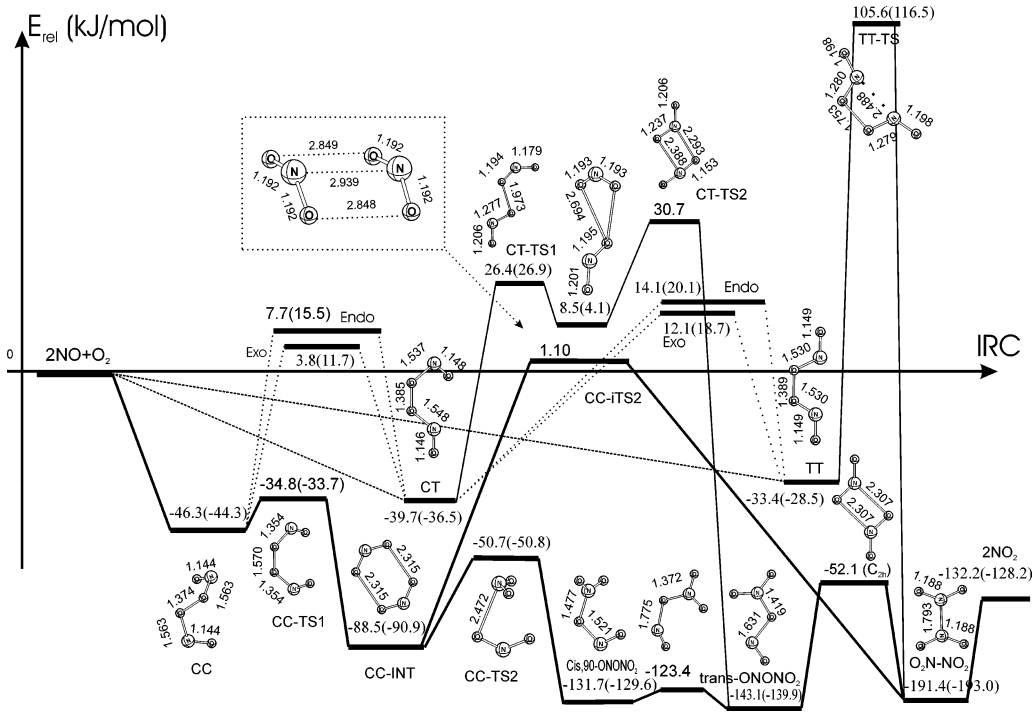

Figure 1. Profile of the singlet PES for the thermal reaction $2NO + O_2 \rightarrow 2NO_2$, obtained at the level UB3LYP/6-311+G(2d) in this study. The dotted and solid lines indicate the minimum energy pathways. Bond lengths are in Å; relative enthalpies are in kJ/mol. Values in parentheses taken from ref 24 are at the B3LYP/6-311G* level.

TABLE 1: Total Energies of Singlet Stationary Points, Optimized with Different DFT Functionals and 6-311+G(2d) Basis Set

system	B3LYP *E*, au	B3LYP *E*, au	TPSS *E*, au	VSXC *E*, au	PBE *E*, au	BP86 *E*, au
	aug-pc3			6-311+G(2d)		
O_2	−150.399229	−150.374660	−150.396718	−150.416526	−150.234046	−150.384366
2NO	−259.911121	−259.868534	−259.907526	−259.940472	−259.606995	−259.880133
$2NO + O_2$	−410.310349	−410.243194	−410.304244	−410.356998	−409.841040	−410.264499
$2NO_2$	−410.360676	−410.291924	−410.370295	−410.415572	−409.922802	−410.341701
trans,*trans*-ONOONO(TT)	−410.322876	−410.255526	−410.341802	−410.381638	−409.892516	−410.312956
TT-TS	−410.271795	−410.204241	−410.294026	−410.333922	−409.847492	−410.266761
O_2NNO_2	−410.381986	−410.313733	−410.398549	−410.445742	−409.958404	−410.375047
cis,*trans*-ONOONO(CT)	−410.324774	−410.257812	−410.345397	−410.388733	−409.895870	−410.316257
CT-TS1	−410.301085	−410.233429	−410.328812	*a*	*a*	*a*
CT-INT	−410.308091	−410.240027	*a*	−410.392236	−409.937331	*a*
CT-TS2	−410.300469	−410.231870	−410.324539	−410.376501	−409.883383	−410.300468
trans-$ONONO_2$	−410.363562	−410.295972	−410.377848	−410.421359	−409.933299	−410.351736
cis,*cis*-ONOONO(CC)	−410.326884	−410.260264	−410.349705	−410.401668	−409.900192	−410.320476
CC-TS1	−410.323064	−410.256033	−410.342557	−410.389129	−409.894185	−410.313891
CC-INT	−410.343333	−410.275834	−410.373221	−410.426173	−409.932114	−410.349331
CC-TS2	−410.329677	−410.261894	−410.358303	−410.420036	−409.918393	−410.335243
cis,90-$ONONO_2$	−410.359304	−410.291747	−410.379058	−410.426469	−409.937343	−410.354822
CC-CT-TS1 (exo)	−410.308522	−410.241771	−410.329763	−410.376089	−409.879018	−410.299768
CC-CT-TS2 (endo)	−410.307111	−410.240356	−410.328154	−410.376212	−409.877444	−410.298135
CT-TT-TS1 (exo)	−410.305582	−410.238520	−410.324351	−410.364629	−409.873584	−410.294397
CT-TT-TS2 (endo)	−410.305031	−410.237998	−410.324006	−410.366232	−409.873336	−410.294072
TS-cc-iTS2	−410.310969	−410.242790	−410.342431	−410.400509	−409.902718	−410.319309
TS-*cis*−*trans*-$ONONO_2$	−410.356139	−410.288710	−410.370229	−410.417749	−409.925080	−410.343532
TS-O_2NNO_2-i-*trans*-$ONONO_2$	−410.330409	−410.262391	−410.357282	*a*	*a*	−410.333196
TS-CC-i-CT	−410.304579	−410.237536	−410.328964	−410.367849	−410.299496	−410.299496

[a] Structure does not exist at this theory level.

optimized local minima on PES are given in Figure 1. Table 2 provides relative energies ΔE and enthalpies of reactions $2NO + O_2 \rightarrow X$ at zero temperature ΔH^0(0 K, $2NO + O_2 \rightarrow X$), where X is a stationary point. Detailed information is collected in the Supporting Information.

In the present work, we report several new transition states (Figure 1; two local minima are mentioned to define TS): **CC-INT** ↔ O_2NNO_2 (D_{2h}); *cis*,90-$ONONO_2$ ↔*trans*-$ONONO_2$; *trans*-$ONONO_2$ ↔ O_2NNO_2 (D_{2h}); **CT-INT** ↔ *trans*-$ONONO_2$; in minor channel − *s-cis*−*cis*-ONOONO → **i-TS** → *s-cis*−*trans*-ONOONO; as well as TS for degenerate isomerization (**CC-TS2a**) and between enantiomers *cis*,90-$ONONO_2$(+) ↔ *cis*,90-$ONONO_2$(−). Their geometric parameters are given in Figure 1 (calculation at the level B3LYP/6-311+G(2d)). The detailed table of geometric parameters for different theory levels is provided in the Supporting Information.

Stability analysis shows that intermediates **CC-INT** and **CT-INT** (see Figure 1), when they exist at the given theory level, display singlet−triplet instability of the Kohn−Sham determinant. At the VSXC/6-311+G(2d) theory level, the intermediate

TABLE 2: Energies and Reaction Enthalpies 2NO + O_2 → X at 0 K, Calculated on the Basis of Different Quantum Chemical Methods

	B3LYP				TPSS	
	aug-pc3		6-311+G(2d)		6-311+G(2d)	
system	E_{rel}, kJ/mol	ΔH^0(0 K), kJ/mol	E_{rel}, kJ/mol	ΔH^0(0 K), kJ/mol	E_{rel}, kJ/mol	ΔH^0(0 K), kJ/mol
$2NO_2$	−136.5	−123.8	−132.2	−119.7	−179.2	−167.1
trans,*trans*-ONOONO(TT)	−34.0	−17.5	−33.5	−17.1	−101.9	−86.8
TT-TS	104.6	116.5	105.7	117.3	27.7	37.4
O_2NNO_2	−194.3	−166.6	−191.4	−163.8	−255.8	−230.1
cis,*trans*-ONOONO(CT)	−39.1	−22.5	−39.7	−23.1	−111.6	−96.1
CT-TS1	25.1	38.1	26.5	39.2	−66.6	−55.1
CT-INT	6.1	21.1	8.6	23.5	*a*	*a*
CT-TS2	26.8	45.4	30.7	49.1	−55.1	−37.2
trans-$ONONO_2$	−144.4	−122.2	−143.2	−121.2	−199.7	−178.9
cis,*cis*-ONOONO(CC)	−44.9	−28.1	−46.3	−29.5	−123.3	−106.9
CC-TS1	−34.5	−20.2	−34.8	−20.5	−103.9	−91.1
CC-INT	−89.5	−70.6	−88.5	−69.7	−187.1	−168.4
CC-TS2	−52.4	−35.2	−50.7	−33.6	−146.7	−129.9
cis,90-$ONONO_2$	−132.8	−111.9	−131.7	−110.8	−203.0	−182.3
CC-CT-TS1 (exo)	5.0	19.1	3.9	17.9	−69.2	−56.0
CC-CT-TS2 (endo)	8.8	22.9	7.7	21.7	−64.9	−51.8
CT-TT-TS1 (exo)	12.9	27.0	12.7	26.6	−54.5	−42.1
CT-TT-TS2 (endo)	14.4	28.5	14.1	28.1	−53.6	−41.1
TS-cc-iTS2	−1.7	12.5	1.1	15.1	−103.6	−90.3
TS-*cis*-i-trans-$ONONO_2$	−124.2	−102.5	−123.5	−101.9	−179.0	−165.7
CC-TS3	−54.4	−36.5	−52.1	−32.1	−143.9	−124.2
TS-CC-i-CT	15.7	32.0	15.4	31.6	−67.1	−51.2

[a] Stationary point does not exist at this theory level.

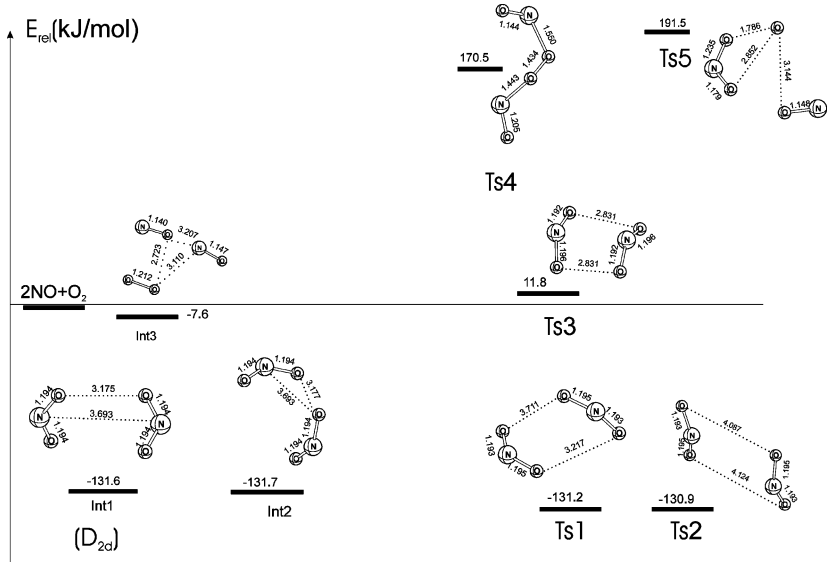

Figure 2. Energy diagram for the stationary points on the triplet PES. Bond lengths are indicated in angstroms; the relative enthalpies are in kJ/mol.

CT-INT has Kohn−Sham determinant with internal instability. The determinant of transition states **CT-TS1**, **CC-TS2** and **CC-TS2a**, **CT-TS2** displays singlet−triplet instability, and the determinant of **CC-iTS2** has internal and singlet−triplet instability at the levels B3LYP/6-311G(d) and B3LYP/6-311+G(2d). These facts indicate low in energy triplet state and may suggest intersystem crossing to the triplet state in the corresponding PES areas.

Because spin conversion is a possible competitive channel of the studied reaction, the parts of triplet PES were also investigated (see Figure 2). Calculations were made at the B3LYP/6-311G(d) theory level and led to new stationary points. Energies and thermodynamic parameters of stationary points discovered on the triplet PES are reported in Table 3. Their geometries are shown in Figure 2.

TABLE 3: Total Energies and Thermodynamic Parameters of Stationary Points on the Triplet PES, Calculated at UB3LYP/6-311G* Theory Level

system	E_{tot}, au	E_{rel}, kJ/mol	Δ,H^0(0 K), kJ/mol
O_2	−150.374660		
2NO	−259.868534		
2NO + O_2	−410.243194	0	0
Int1	−410.266718	−131.6	−138.0
Int2	−410.266749	−131.7	−138.1
Int3	−410.220998	−7.6	−24.2
Ts1	−410.266508	−131.1	−137.9
Ts2	−410.266481	−131.0	−137.9
Ts3	−410.213825	11.9	5.3
Ts4	−410.155342	170.5	159.2
Ts5	−410.147678	191.3	174.8

TABLE 4: Vibration Frequencies in NO, O_2, NO_2, and N_2O_4 Calculated at Different Theory Levels Compared to Experimental Data from Reference 43

symm	B3LYP	B3LYP	TPSS	VSXC	PBE	BP86	experiment
	aug-pc3		6-311+G(2d)				
			NO				
Σ	1974	1955	1872	1911	1859	1872	1904
			O_2				
Σ_g	1638	1629	1544	1574	1536	1550	1580
			NO_2				
A_1	769	761	736	749	733	737	750
A_1	1392	1381	1317	1346	1313	1325	1318
B_2	1695	1672	1599	1644	1606	1632	1618
			N_2O_4				
A_u	88	87	83	90	84	83	82
B_{2u}	225	227	178	222	192	188	265
A_g	293	293	258	278	262	260	265
B_{3u}	444	443	391	387	397	393	425
B_{3g}	497	497	450	461	456	451	480
B_{2g}	702	704	636	644	641	634	657
B_{1u}	763	758	721	721	725	721	755
A_g	851	843	814	819	813	810	807
B_{1u}	1305	1298	1242	1265	1256	1244	1261
A_g	1448	1437	1392	1418	1398	1388	1383
B_{3g}	1785	1765	1699	1752	1723	1702	1718
B_{2u}	1817	1798	1729	1782	1753	1731	1757

3.2. The Choice of Exchange-Correlation Functional. To select the DFT functional providing the most reliable description of thermochemical and activation parameters, we compared the calculated (harmonic) and experimental[36] vibration frequencies of some N- and O-containing molecules (Table 4) as well as the reaction enthalpies $\Delta_r H^0(2NO + O_2 \rightarrow 2NO_2)$ and $\Delta_r H^0(2NO_2 \rightarrow N_2O_4)$ at $T = 0$ K (Table 5). One can see from Tables 4 and 5 that values from quantum chemical calculations at the B3LYP/6-311+G(2d), B3LYP/*aug-pc3*, and TPSS/6-311+G(2d) levels are in better agreement with corresponding experimental data[43,44] that are in accord with single point energy calculations CCSD(T)/aug-cc-pVDZ (see Table 7). The agreement between the calculated and experimental enthalpies[44] of reaction $2NO_2 \rightarrow N_2O_4$ for B3LYP and TPSS functionals is excellent, which allows us to choose them as quantitatively correct calculation of energy and activation enthalpies. Agreement with experimental[44] value $\Delta_r H^0(2NO + O_2 \rightarrow 2NO_2)$ is worse than in case of dimerization reaction $2NO_2 \rightarrow N_2O_4$. Consequently, we find it necessary to make an empirical correction for all of the calculated enthalpies of reactions $2NO + O_2 \rightarrow X$, where X is a stationary point on the singlet PES. The value of this correction Δ is defined as a difference between the experimental and calculated value for $\Delta_r H^0(2NO + O_2 \rightarrow 2NO_2)$.

In the following text, we discuss the values calculated at the B3LYP/*aug-pc3* level, unless specified otherwise, as well as these corrected values of the reaction enthalpies.

Formation of *cis*−*cis*-ONOONO ($\Delta_r H^0(2NO + O_2 \rightarrow$ ONOONO) = −10.1 kJ/mol) presents the first stage in the first reaction channel. This intermediate isomerizes with a little (10.4 kJ/mol) activation energy into a flat cyclic structure **CC-INT** (point group D_{2h}). Intermediate **CC-INT** on the singlet PES can undergo, apart from homolysis **CC-INT** → $2NO_2$, two monomolecular transformations **CC-INT** → O_2NNO_2 and **CC-INT** → *cis*-$ONONO_2$ through either a high-energy TS **CC-iTS2** (E_a = 87.8 kJ/mol) or a low-energy TS **CC-TS2** (E_a = 37.0 kJ/mol). This high-energy reaction channel had not been considered earlier. It is possible that the barrier height (87.8 kJ/mol) of **CC-INT** → O_2NNO_2 activation reaction is overestimating the true value, due to internal instability in the Kohn−Sham determinant of TS **CC-iTS2**.

Intermediate *cis*-$ONONO_2$ isomerizes (E_a = 8.6 kJ/mol), forming a more stable ($\Delta_r H^0$ = −10.4 kJ/mol) intermediate *trans*-$ONONO_2$, which further retransforms to O_2NNO_2 with activation energy E_a = 54.4 kJ/mol. Despite our efforts to find a TS of *cis*-$ONONO_2$ → O_2NNO_2 reaction, a saddle point on the singlet surface was not found. It appears that this reaction cannot proceed in one step. Elementary reactions *cis*-$ONONO_2$ → *trans*-$ONONO_2$ and *trans*-$ONONO_2$ → O_2NNO_2 need to be added to the mechanism suggested by Olson et al.[24] The TSs of these steps are lower in energy than in the initial reactant, which is an argument in favor of this mechanism. Analysis of the energetic reaction profile (Figure 1) allows us to conclude that the energy of the highest TS in the reaction main channel relative to initial reagents has a negative value (−34.8 kJ/mol). The corresponding enthalpy $\Delta H^{\ddagger}(2NO + O_2 \rightarrow$ **CC-TS1**) makes −20.2 kJ/mol. However, after the above considered empirical correction of calculated enthalpies of reactions $2NO + O_2 \rightarrow X$, where X is a stationary point on a singlet PES, for the additive value Δ the reaction activation enthalpy (1) is $\Delta H^{\ddagger}$ = −4.5 kJ/mol. This value agrees with the experimental (Arrhenius) activation energy (−4.5 kJ/mol) within the temperature range between 298 and 600 K.

Among considered conformers of the primary intermediate, the *cis*−*cis* conformer is the most energetically favorable, followed by *cis*−*trans* (6.6 kJ/mol higher in energy), and *trans*−*trans* (6.3 kJ/mol higher in energy than *cis*−*trans*).

3.3. Singlet Potential Energy Surface. The two-dimensional section of PES corresponding to the homolysis of *s-cis*−*cis*-ONOONO is shown in Figure 3. This reaction is the reverse of the first elementary step in the mechanism of ref 24. We selected the distance ON−OO as a reaction coordinate and scanned it from 1.2 to 3.5 Å. All of the remaining degrees of freedom were optimized. Orientation of the NO fragment was changed to the one opposite to the central fragment (O−O), but that did not result in any significant energy change, and the PES remained smooth. The PES profile remains symmetrical relative to the bisector surface that corresponds to C_2 point group symmetry of the initial geometry for the *s-cis*−*cis*-ONOONO molecule and symmetric dissociation of the fragments NO···OO···ON.

The singlet adiabatic PES in Figure 3 allows us to state that other intermediates and TS are absent at the stage of thermal association $2NO + O_2 \rightarrow$ *cis*−*cis*-ONOONO. We can assume that a similar situation takes place when forming other conformers of the primary intermediate: $2NO + O_2 \rightarrow$ *cis*−*trans*-ONOONO and *trans*−*trans*-ONOONO. Thus, formation of ONOONO is the initial stage of the oxidation process, and other intermediates are absent on the PES corresponding to the reaction $2NO + O_2 \rightarrow$ ONOONO.

To investigate the PES topology, we computed internal reaction coordinates (IRC) with additional parameters set, affecting PES scanning. Spin states were controlled during scanning, where the spin square $\langle \hat{S}^2 \rangle$ value before and after annihilation served as an indicator of spin-contamination. Spin-contaminated states were found at steps **CT-TS2** → *trans*-$ONONO_2$ and **CC-iTS2** → O_2NNO_2.

Following the IRC curve out of **CC-TS2** (Figure 4) to the side opposite to *cis*-$ONONO_2$ (reactant valley) led to a new saddle point, which was identified as the TS of **CC-INT** isomerization (rotation of two ONO fragments relative to *N*−*N*

TABLE 5: Enthalpy of Reactions 1 and 2 (kJ/mol) Evaluated at Different DFT Levels and Compared to the Experimental Data from Reference 44

reaction	B3LYP	B3LYP	TPSS	VSXC	PBE	BP86	experiment
	aug-pc3			6-311+G(2d)			
$2NO + O_2 \rightarrow 2NO_2$	−123.82	−119.70	−167.12	−146.46	−209.28	−197.18	−105.55
$2NO_2 \rightarrow N_2O_4$	−42.81	−44.09	−62.96	−67.7	−82.76	−76.71	−53.60

axis), conserving C_s mirror plane. This TS, referred to as **CC-TS2a**, was not mentioned previously.[24,25]

This descent path from the transition state is not to a local minimum, but to another transition state as a consequence[45] of a bifurcation point[46] on the PES (valley-ridge inflection point, VRI). This type of potential energy surface is a mechanism different from both stepwise and concerted mechanisms and is known as a two-step no-intermediate mechanism. Recently,[45] there was a discussion of the role of VRI the reaction mechanisms. Presently, there are enough examples of identified VRI points, mostly for organic compound reactions (see works[48,45,49] and references therein). Until now, these points were not reported for reaction 1. Examples of VRI points with other inorganic reactions are rare.[50−52]

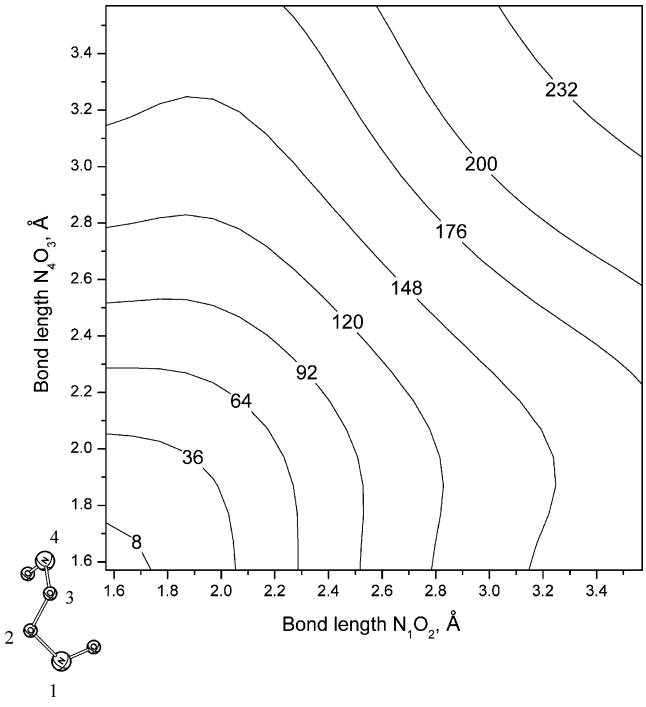

Figure 3. Two-dimensional singlet state potential energy surface scan along two N−O bond lengths in peroxide *cis*−*cis*-$ON_1-O_2O_3-N_4O$. All other degrees of freedom were optimized. Energy contour values are calculated at the B3LYP/6-311G* theory level and reported in kJ/mol relative to the *s-cis*−*cis*-ONOONO conformation.

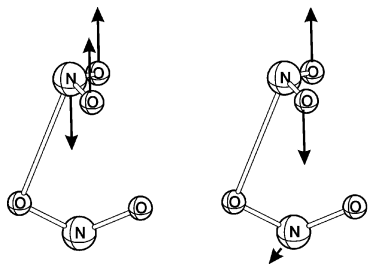

Figure 4. Symmetrical (left) and anti-symmetrical (right) vibration modes of **CC-TS2** that interchange imaginary value along the IRC curve.

This VRI point is a point on the PES where the Hessian matrix has a zero eigenvalue, and the corresponding eigenvector is perpendicular to the gradient.[46] This unusual PES topology led to the IRC curve not being the reaction path after the bifurcation point (VRI), as the figurative point moves dynamically unstable along the tangent of the PES ridge. IRC curve is the steepest descent path and MEP before the bifurcation point, but begins to deviate thereafter. The VRI point is not the critical point on the IRC curve. Additional mathematical details can be found in refs 53−55.

We performed analysis of harmonic frequencies and corresponding movements of atomic nuclei to find the VRI point on the IRC curve, which was composed of a small step size of 0.01 amu$^{1/2}$ bohr. Figure 5 shows the change of the two vibration modes, taking imaginary values at sequential TSs connected by the IRC curve (**CC-TS2** and **CC-TS2a**).

Descent along the IRC curve from **CC-TS2** is accompanied by a decrease of surface curvature in the direction orthogonal to the IRC, and a decrease in the absolute value of the antisymmetric vibration frequency mode (dashed line at Figure 5), which destroys the planar C_s symmetry. The point where this frequency becomes zero corresponds to the transformation of the valley into the ridge or valley-ridge; a inflection (VRI) point. This is the bifurcation point of the MEP, where the reaction path splits into two degenerate fluxes. According to the recent classification,[56] the present VRI point is valley-pitchfork VRI (vp-VRI), the point dividing identical reagent valleys.

When the coordinate system was changed from mass-weighted to Cartesian coordinates, the IRC curve plotted from **CC-TS2** in the opposite direction to *cis*-$ONONO_2$ (reagents valley) led to the cyclic intermediate **CC-INT**. Thus, the IRC curve in mass-weighted internal coordinates is different from the IRC curve in Cartesian coordinates. This fact does not undermine the existence of the VRI point, because the bifurcation point on the reaction path is a physically observed property of the PES.[45,47,57−61] The existence of a continuous IRC curve

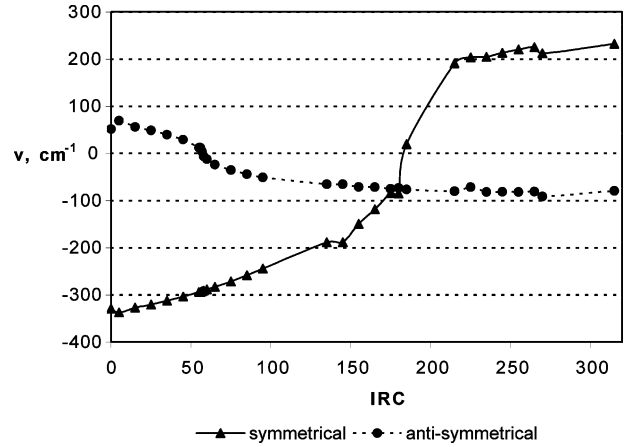

Figure 5. Behavior of vibration modes corresponding to the imaginary frequencies in the two sequential transition states along the IRC curve: saddle points **CC-TS2** and **CC-TS2a**.

TABLE 6: Total (E_{tot}, au) and Relative (E_{rel}, kJ/mol) Energies of Intermediates Calculated at Level UCCSD/6-311G* and Corresponding Value of T_1-Test

system	total energy, au	E_{rel}	T_1
$2NO + O_2$	−409.256628	0	
CC	−409.263836	−19.6	0.0249
CT	−409.262145	−14.9	0.0244
TT	−409.260541	−10.6	0.0237
CC-INT	−409.247629	24.4	0.0231
cis,90-$ONONO_2$	−409.291320	−94.1	0.0231
trans-$ONONO_2$	−409.295613	−105.8	0.0220

between **CC-TS2** and *cis*-$ONONO_2$ confirms the existence of reaction path **CC-INT** → **CC-TS2** → *cis*-$ONONO_2$, which was suggested by Olson et al.[24]

3.4. Triplet Potential Energy Surface. Singlet−triplet instability of the KS determinant was found for intermediates **CC-INT** (in main channel), **CT-INT** (in minor channel), and saddle points **CT-TS1**, **CC-TS2**, **CT-TS2**, **CC-iTS2**, as well as **CC-TS2a** (TS of degenerate isomerization of **CC-INT**). This may be indicative of a triplet state lower in energy than the singlet for these species. To verify this notion, we completed a search for the stationary points on the triplet PES.

The stationary points found are presented in Figure 2. The energies of the local minima and TSs are given in Table 3. Kohn−Sham determinants of all of the stationary points on the triplet PES are stable. All found intermediates and TS have floppy structures, with the lowest vibration frequency not exceeding 100 cm^{-1}. Thus, triplet PES of nitrous oxides has small energy gradients over comparatively large areas, which complicated other quantum chemical studies of the nitride oxides.[16−19,65]

Intermediate *cis*−*cis*-ONOONO underwent fragmentation on triplet PES with terminal NO groups moving away to ∼3 Å distance from the OO′ fragment during optimization. This fact allows us to conclude that initial reaction steps occur on the singlet PES. For all stationary points on the triplet PES, we found that the bond lengths of the NO_2 fragments are close to values in isolated NO_2 ($^2A_1$) radical. Therefore, the local minima and transition states on the triplet PES are closer to reaction products than to reactants.

Hence, we can assume that the thermal reaction $2NO + O_2 \rightarrow 2NO_2$ may proceed on the triplet PES at the final reaction steps. Presumably, this happens in the vicinity of the **CC-INT** intermediate, which presents the "earliest" structure in the reaction main channel with a singlet−triplet instability. If the rate of singlet−triplet internal conversion is high enough, this channel can compete with the main reaction channel, connecting **CC-INT** and O_2NNO_2.

3.5. Comparison of DFT with Correlated Wave Function Theory Methods. Several intermediates, including *s-cis*−*cis*-ONOONO, *s-cis*−*trans*-ONOONO, *s-trans*−*trans*-ONOONO, and **CC-INT**, were found to have nearly degenerate electronic energy levels. This casts the shade of doubts on the previously published energy values, which were obtained using MP2,[22,23] CBS-QB3,[24] and QCISD(T)[21] methods. To investigate this further, we carried out complete optimization at UCCSD/6-311G(d) level and used the T_1-test[62] to establish the significance of nondynamic correlation. A value of $T_1 > 0.02$ typically indicates[62] that nondynamic correlation is strong and single reference methods may be unreliable. From the results presented in Table 6, one can see that the T_1 value indicates strong nondynamic electron correlation in all cases. As one can see from comparison of Tables 6 and 2, the relative energies for all intermediates, calculated at UCCSD/6-311G* theory level, differ significantly from the values obtained with DFT. The apparent controversy is resolved by results obtained at UCCSD(T)/aug-cc-pVDZ//B3LYP/aug-pc3 theory level, presented in Table 7. The relative energies changed dramatically from the UCCSD/6-311G* results and are now in excellent agreement with the B3LYP/aug-pc3 values. It is believed[62] that results of the CCSD(T) method are meaningful while $T_1 < 0.04$, a condition that is satisfied for all of the stationary points considered.

On the other hand, the results presented in Table 7 indicate that the relative energies of **CC-INT** calculated at both RI-B2PLYP/aug-cc-pVDZ (−137.1 kJ/mol) and B2K-LYP/aug-cc-pVDZ (−121.7 kJ/mol) theory levels are different from both B3LYP/aug-pc3 (−89.5 kJ/mol) (see Table 2) and CCSD(T)/aug-cc-pVDZ (−86.6 kJ/mol). Thus, intermediate **CC-INT** is more energetically favorable at the double hybrid DFT level. For the other stationary points (excluding **CC-TS2**, TS-O_2NNO_2-i-*trans*-$ONONO_2$, and **CC-iTS2**), relative energy values are in excellent agreement both with conventional DFT and double hybrid DFT functionals. The stationary point **CC-iTS2** does not exist at both RI-B2PLYP/aug-cc-pVDZ and B2K-LYP/aug-cc-pVDZ levels. The relative energies of stationary points **CC-TS2** and **CC-TS3** calculated at the double hybrid levels decreased in comparison with both UCCSD(T) and UB3LYP calculations. The O−N bond length in the NON fragment (the distance between two adjacent NO_2 groups) decreased no more than 0.4 Å in double hybrid calculations in comparison with optimization at the level UB3LYP/aug-pc3. For **CC-TS3**, this distance increased by 0.5 Å. The corresponding relative energies decrease significantly in comparison with both UCCSD(T) and UB3LYP values.

The multireference character of a wave function for transition states and intermediates can be verified by CAS-SCF calculations in a sufficiently large active space. McKee[21] made an earlier attempt to optimize the **TT** intermediate geometry with the CAS-SCF method. He assumed that the appropriate active space needed to include two NO π-orbitals, two NO π^*-orbitals, three σ-orbitals for describing N−O−O−N peroxide fragment, and three σ^*-orbitals. We performed geometry optimization of the conformers **CC**, **CT**, **TT** and transition states **CC-TS1**, **CC-TS2**, and **TT-TS** with a similar active space at CAS(10,10)/6-311G* and CAS(10,10)/6-311+G(2d) theory levels. We also considered other choices of the active space: CAS(4,4) with two bonding π-orbitals NO, two antibonding π^*-orbitals NO, CAS(14,12) where two bonding σ-orbitals NO were added to McKee[21] active space, and CAS(26,16) where all valence electrons are correlated on two antibonding π^*-orbitals of NO and one antibonding σ^*-orbital of OO fragments.

CASSCF solutions for all of the mentioned active spaces of **CC** had broken symmetry for both wave function and optimized nuclear configuration. Electronic structure analysis indicated orbital "intrusion", where the orbitals excluded from the active space in the initial guess, based on chemical assumptions, appear in the active space after CASSCF orbital optimization. This may indicate an incorrect choice of the active space, as suggested in ref 21. Further increase in the active space was found to be unfeasible, as it generates more than 3×10^7 determinants. CASSCF(26,16) solution for **TT** and O_2NNO_2 had correct symmetry of nuclei configurations (C_{2v} and D_{2h}, respectively). The geometries of saddle point **TT-TS** and intermediate **CC-INT** were optimized at the level CAS(26,16)/6-311G(d), and the located stationary points were characterized by vibrational frequency calculations. In the optimized structures (see Figure 6), the O−O bond length in cyclic **CC-INT** is increased to ca. 3 Å; the vibration mode corresponding to O−O bonds stretching

TABLE 7: Relative (E_{rel}, kJ/mol) Energies of Intermediates and Transition States Calculated at Different Theory Levels

system	E_{rel}, kJ/mol	E_{rel}, kJ/mol	E_{rel}, kJ/mol	E_{rel}, kJ/mol
	B3LYP (BS-B3LYP) 6-311+G(2d)	RI-B2PLYP	B2K-PLYP aug-cc-pVDZ	CCSD(T)
$2NO_2$	−132.2	−132.9	−122.4	−92.5
O_2NNO_2	−191.4	−193.5	−184.3	−155.6
trans,*trans*-ONOONO(TT)	−33.5	−31.3	−17.3	−31.6
cis,*trans*-ONOONO(CT)	−39.7	−40.1	−25.7	−38.8
TT-TS	105.6	108.7	130.3	107.4
trans-$ONONO_2$	−143.2	−145.1	−136.8	−130.5
cis,*cis*-ONOONO(CC)	−46.3	−50.7	−35.7	−46.9
CC-TS1	−34.8	−33.8	−17.9	−29.2
CC-INT	−88.5 (−134.6)	−137.1	−121.7	−86.8
CC-TS2	−50.7 (−133.3)	−98.5	−80.9	−71.1
cis,90-$ONONO_2$	−131.7	−133.6	−125.2	−113.1
TS-cc-iTS2	*a*	*a*	*a*	−58.4
TS-*cis*-i-*trans*-$ONONO_2$	−123.5	−126.6	−119.4	−112.3
CC-TS3	−52.1	−73.2	−49.7	−45.7

[a] Stationary point does not exist at this theory level.

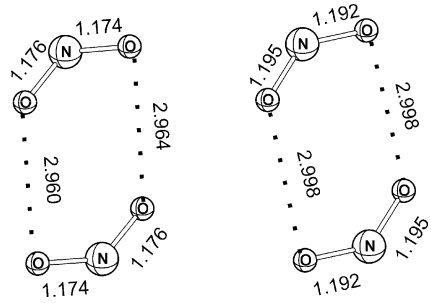

Figure 6. Geometries of intermediate **CC-INT** optimized at the levels CAS(26,16)/6-311G(d) (left) and BS-UB3LYP/6-311+G(2d) (right).

TABLE 8: Total (E_{tot}, au) and Relative (E_{rel}, kJ/mol) Energies of Stationary Points Optimized at the Level CAS(26,16)/6-311G*

stationary point	E_{tot}, au	E_{rel}, kJ/mol
O_2NNO_2	−408.324150	0.0
TT	−408.266120	157.4
TT-TS	−408.239740	229.0
CC-INT	−408.314480	26.2

has the low value (65 cm^{-1}). Thus, geometry optimization at the level CAS(26,16)/6-311G(d) leads to gas-phase cluster of two weakly bound NO_2 radicals (Table 8).

Because even the largest active space (26,16) is not flexible enough for all of the stationary points, we conclude that the CASSCF results described above should be considered only as qualitative. It is known (see articles[47,46] and references therein) that the broken-symmetry DFT[63,64] approach can be accurate in describing a diradicaloid system. Because several stationary points could be singlet diradicals, we performed geometry optimization of stationary points in the main channel at the BS-B3LYP/6-311+G(2d) theory level. The obtained relative energies changed only for two stationary points, **CC-INT** and **CC-TS2**, and they are shown in Table 7 in parentheses. Atomic configurations and geometrical parameters are shown in Figure 6.

Not surprisingly, the results of the BS-B3LYP/6-311+G(2d) optimization for **CC-INT** were found to be similar to the CASSCF structures: the difference of O−O bond lengths is 0.037 Å (2.961 and 2.998 Å for CASSCF and BS-B3LYP, respectively); the difference of NO bond lengths is no more than 0.019 Å. The energy difference between **CC-INT** and O_2NNO_2 at the BS-B3LYP/6-311+G(2d) theory level is 56.8 kJ/mol, a decrease in a comparison with the UB3LYP/aug-pc3 value (102.9 kJ/mol), and is closer to the CAS(26,16) result (26.2 kJ/mol). The largest differences were found in geometrical parameters and relative energies for two structures optimized with BS-DFT and DFT approaches: for **CC-INT** (O−O bond was elongated to almost 3 Å), and for **CC-TS2** (O···N bond length was elongated to 2.9 Å, and the point group decreased from C_s to C_1). For both stationary points, relative energy decreased to −130 kJ/mol. The relative energy of **CC-INT** calculated at the BS-B3LYP/6-311+G(2d) level is very close to the value calculated at the double hybrid DFT level. The **CT-TS2** and **CC-iTS2** do not exist at this level. The stability order of 2NO + O_2, **CC**, **CC-TS1**, and **CC-INT** remains the same at all levels used (DFT, BS-DFT, and double hybrid DFT).

On the basis of the results described above, we conclude that the stability of the ONOONO conformers decreases in the following order: *s-cis*−*cis*-ONOONO (**CC**), *s-cis*−*trans*-ONOONO (**CT**), and *s-trans*−*trans*-ONOONO (**TT**). Intermediates **CC-INT**, **CC**, **CT**, and **TT** energies are lower than isolated reagents energy (2NO + O_2). It should be noted that the barrier heights obtained with DFT agree well with the observed negative temperature dependence of the rate constant for reaction 1.

4. Conclusions

We reported the detailed analysis of the singlet and triplet potential energy surfaces for the reaction between molecular oxygen and two nitric oxide molecules. We used a range of methods, including DFT (B3LYP, TPSS, VSXC, BP86, PBE), double hybrid DFT (RI-B2PLYP, B2K-LYP), CASSCF, and coupled cluster theory. We studied elementary steps involving various N_2O_4 isomers, including *cis*−*cis*-, *cis*−*trans*-, *trans*−*trans*-ONOONO, *cis*- and *trans*-$ONONO_2$, O_2NNO_2, as well as Coupe-type quasi-aromatic hexagonal ring intermediate **CC-INT**, and van-der-Waals molecular clusters. T_1-test values in CCSD calculations evidence strong nondynamic electron correlation, but electronic structure in the CASSCF method is plagued by the presence of intruder states. Both BS-UDFT and CASSCF results suggest that **CC-INT** proposed by Olson et al. is probably not a key intermediate determining the separate elementary step, but rather a weakly bound "product-like" molecular cluster.

Among DFT methods, B3LYP/aug-pc3, B3LYP/6-311+G(2d), and TPSS/6-311+G(2d) theory levels appear to be the most

SCHEME 2: Four Key Intermediates of the Reaction: (a) *cis*,90-ONONO$_2$; (b) *trans*-ONONO$_2$; (c) *cis*,*cis*-ONOONO; (d) CC-INT

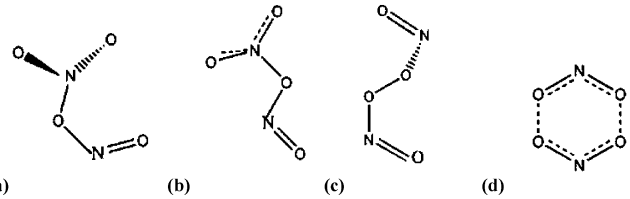

reliable, based on comparison of the experimental and estimated enthalpy for the NO_2 dimerization reaction. According to results obtained at these theory levels, the main channel of reaction $2NO + O_2 \rightarrow 2NO_2$ is through the following reactions (values are given for B3LYP/aug-pc3):

$$2NO + O_2 \rightarrow cis{-}cis\text{-ONOONO}$$
$$(\Delta_r H = -10.1\ \text{kJ/mol}, E_a = 0\ \text{kJ/mol})$$
$$cis{-}cis\text{-ONOONO} \rightarrow \text{TS1} \rightarrow NO_2{\cdot}O_2N$$
$$(\Delta_r H = -42.5\ \text{kJ/mol}, E_a = 10.4\ \text{kJ/mol})$$
$$NO_2{\cdot}O_2N \rightarrow \text{TS2} \rightarrow cis\text{-ONONO}_2$$
$$(\Delta_r H = -41.3\ \text{kJ/mol}, E_a = 37.8\ \text{kJ/mol})$$
$$cis\text{-ONONO}_2 \rightarrow \text{TS3} \rightarrow trans\text{-ONONO}_2$$
$$(\Delta_r H = -10.4\ \text{kJ/mol}, E_a = 8.6\ \text{kJ/mol})$$
$$trans\text{-ONONO}_2 \rightarrow \text{TS4} \rightarrow O_2NNO_2$$
$$(\Delta_r H = -44.4\ \text{kJ/mol}, E_a = 90.0\ \text{kJ/mol})$$

The structures of the key intermediates are drawn in Scheme 2.

Overall, the activation enthalpy of the reaction $2NO + O_2 \rightarrow 2NO_2$ at absolute zero $\Delta H^{\ddagger}(0\ \text{K})$, evaluated at B3LYP/*aug-pc3* and B3LYP/6-311+G(2d) theory levels, corrected by the value of the reaction enthalpy, equals −4.5 and −6.5 kJ/mol, respectively. This agrees with the experimental value E_a of −4.5 kJ/mol at $T = 298-600$ K and $E \approx 0$ kJ/mol at $T \approx 650$ K.

Acknowledgment. This work is supported in part by the Russian Foundation for Basic Research (project no. 07-03-00390), and by the U.S. National Science Foundation (CCF-0740344, and CHE-0832622). O.B.G. is thankful to Sergey N. Ruzheinikov from the Krebs Institute for Biomolecular Research, Department of Molecular Biology and Biotechnology, for helpful discussions. A.E.M. would like to thank the UCF Institute of Simulation and Training (IST) Stokes HPCC facility for the generous donation of computer time, and Eugenia A. Vinogradova and James P. Ritchie for their help with the manuscript preparation.

Supporting Information Available: Additional data. This material is available free of charge via the Internet at http://pubs.acs.org.

References and Notes

(1) Gershinowitz, H.; Eyring, H. *J. Am. Chem. Soc.* **1935**, *57*, 985.
(2) Bodenstein, M.; Wachenheim, L. Z. *Z. Elektrochem.* **1918**, *24*, 183.
(3) Bodenstein, M. *Z. Phys. Chem.* **1922**, *100*, 68.
(4) Kassel, L. S. *J. Phys. Chem.* **1930**, *34*, 1777.
(5) Olbregts, J. *Int. J. Chem. Kinet.* **1985**, *17*, 835.
(6) Tsukahara, H.; Ishida, T.; Mayumi, M. *Nitric Oxide: Biol. Chem.* **1999**, *3*, 191.
(7) Cox, R. A.; Coker, G. B. *J. Atmos. Chem.* **1983**, *1*, 53.
(8) Solc, M. *Nature* **1966**, *209*, 706.
(9) Treacy, J. C.; Daniels, F. *J. Am. Chem. Soc.* **1955**, *77*, 2033.
(10) Hisatsune, I. C.; Zafonte, L. *J. Phys. Chem.* **1969**, *73*, 2980.
(11) Hasche, R. L.; Patrick, W. A. *J. Am. Chem. Soc.* **1925**, *47*, 1207.
(12) Bhatia, S. C.; Hall, J. J. H. *J. Phys. Chem.* **1980**, *84*, 3255.
(13) Brown, F. B.; Crist, R. H. *J. Chem. Phys.* **1941**, *9*, 840.
(14) Ashmore, P. G.; Burnett, M. G.; Tyler, B. J. *Trans. Faraday Soc.* **1962**, *58*, 685.
(15) Morris, V. R.; Bhatia, S. C.; Hall, J. J. H. *J. Phys. Chem.* **1990**, *94*, 7418.
(16) Siegbahn, P. E. M. *J. Comput. Chem.* **1985**, *6*, 182.
(17) Eisfeld, W.; Morokuma, K. *J. Chem. Phys.* **2000**, *113*, 5587.
(18) Eisfeld, W.; Morokuma, K. *J. Chem. Phys.* **2001**, *114*, 9430.
(19) Eisfeld, W.; Morokuma, K. *J. Chem. Phys.* **2003**, *119*, 4682.
(20) Lee, E. P. F.; Wright, T. G. *Chem. Phys. Lett.* **2001**, *347*, 429.
(21) McKee, M. L. *J. Am. Chem. Soc.* **1995**, *117*, 1329.
(22) Wang, X.; Qin, Q.-Z.; Fan, K. *J. Mol. Struct. (THEOCHEM)* **1998**, *432*, 55.
(23) Wang, X.; Qin, Q.-Z. *Int. J. Quantum Chem.* **2000**, *76*, 77.
(24) Olson, L. P.; Kuwata, K. T.; Bartberger, M. D.; Houk, K. N. *J. Am. Chem. Soc.* **2002**, *124*, 9469.
(25) Choi, Y. M.; Lin, M. C. Ab initio study on the termolecular reaction of $2NO + O_2$ and the complex self-reaction of NO_2. 6th International Conference on Chemical Kinetics; National Institute of Standards and Technology, Gaithersburg, MD, 25−29 July, 2005.
(26) Frisch, M. J.; Trucks, G. W.; Schlegel, H. B.; Scuseria, G. E.; Robb, M. A.; Cheeseman, J. R.; Montgomery, J. A., Jr.; Vreven, T.; Kudin, K. N.; Burant, J. C.; Millam, J. M.; Iyengar, S. S.; Tomasi, J.; Barone, V.; Mennucci, B.; Cossi, M.; Scalmani, G.; Rega, N.; Petersson, G. A.; Nakatsuji, H.; Hada, M.; Ehara, M.; Toyota, K.; Fukuda, R.; Hasegawa, J.; Ishida, M.; Nakajima, T.; Honda, Y.; Kitao, O.; Nakai, H.; Klene, M.; Li, X.; Knox, J. E.; Hratchian, H. P.; Cross, J. B.; Bakken, V.; Adamo, C.; Jaramillo, J.; Gomperts, R.; Stratmann, R. E.; Yazyev, O.; Austin, A. J.; Cammi, R.; Pomelli, C.; Ochterski, J. W.; Ayala, P. Y.; Morokuma, K.; Voth, G. A.; Salvador, P.; Dannenberg, J. J.; Zakrzewski, V. G.; Dapprich, S.; Daniels, A. D.; Strain, M. C.; Farkas, O.; Malick, D. K.; Rabuck, A. D.; Raghavachari, K.; Foresman, J. B.; Ortiz, J. V.; Cui, Q.; Baboul, A. G.; Clifford, S.; Cioslowski, J.; Stefanov, B. B.; Liu, G.; Liashenko, A.; Piskorz, P.; Komaromi, I.; Martin, R. L.; Fox, D. J.; Keith, T.; Al-Laham, M. A.; Peng, C. Y.; Nanayakkara, A.; Challacombe, M.; Gill, P. M. W.; Johnson, B.; Chen, W.; Wong, M. W.; Gonzalez, C.; Pople, J. A. *Gaussian 03*, D.02 ed.; Gaussian, Inc.: Wallingford, CT, 2007.
(27) Grimme, S. *J. Chem. Phys.* **2006**, *124*, 034108.
(28) Schwabe, T.; Grimme, S. *Phys. Chem. Chem. Phys.* **2007**, *9*, 3397.
(29) Neese, F. *ORCA - An ab initio, DFT and semiempirical SCF-MO package, Version 2.6−63*; April, 2008.
(30) Neese, F.; Olbrich, G. *Chem. Phys. Lett.* **2002**, *362*, 170.
(31) Neese, F.; Wennmohs, F.; Hansen, A.; Becker, U. *Chem. Phys.* **2009**, *356*, 98.
(32) Karton, A.; Tarnopolsky, A.; Lamère, J.-F.; Schatz, G. C.; Martin, J. M. L. *J. Phys. Chem. A* **2008**, *112*, 12868.
(33) Tarnopolsky, A.; Karton, A.; Sertchook, R.; Vuzman, D.; Martin, J. M. L. *J. Phys. Chem. A* **2008**, *112*, 3.
(34) Ignatov, S. K. *Moltran - Program for molecular visualization and thermodynamic calculations*, 2.5 ed.; University of Nizhny Novgorod, 2007; http://ichem.unn.ru/moltran.
(35) Dennington, R. K. T., II; Millam, J.; Eppinnett, K.; Hovell, W. L.; Gilliland, R. GaussView, version 3.09; Semichem, Inc.: Shawnee Mission, KS, 2003.
(36) Curtiss, L. A.; Raghavachari, K.; Redfern, P. C.; Pople, J. A. *J. Chem. Phys.* **2005**, *123*, 124107.
(37) Jensen, F. *J. Chem. Phys.* **2001**, *115*, 9113.
(38) Jensen, F. *J. Chem. Phys.* **2002**, *116*, 7372.
(39) Jensen, F. *J. Chem. Phys.* **2002**, *117*, 9234.
(40) Jensen, F. *J. Chem. Phys.* **2003**, *118*, 2459.
(41) Jensen, F.; Helgaker, T. *J. Chem. Phys.* **2004**, *121*, 3463.
(42) Jensen, F. *J. Phys. Chem. A* **2007**, *111*, 11198.
(43) Huber, K. P.; Herzberg, G. *Molecular Spectra and Molecular Structure. IV. Constants of Diatomic Molecules*; Van Nostrand Reinhold Co.: New York, 1979.
(44) Chase, M. W., Jr.; Davies, C. A.; Downey, J. R., Jr.; Frurip, D. J.; McDonald, R. A.; Syverud, A. N. *J. Phys. Chem. Ref. Data* **1985**, *14*, Suppl. 1.
(45) Ess, D. H.; Wheeler, S. E.; Iafe, R. G.; Xu, L.; Celebi-Olçüm, N.; Houk, K. N. *Angew. Chem., Int. Ed.* **2008**, *47*, 7592.
(46) Valtazanos, P.; Ruedenberg, K. *Theor. Chim. Acta* **1986**, *69*, 281.
(47) Singleton, D. A.; Hang, C.; Szymanski, M. J.; Meyer, M. P.; Leach, A. G.; Kuwata, K. T.; Chen, J. S.; Greer, A.; Foote, C. S.; Houk, K. N. *J. Am. Chem. Soc.* **2003**, *125*, 1319.
(48) Quapp, W.; Hirsch, M.; Heidrich, D. *Theor. Chem. Acc.* **2004**, *112*, 40.
(49) Bettinger, H. F.; Kaiser, R. I. *J. Phys. Chem. A* **2004**, *108*, 4576.
(50) Quapp, W.; Melnikov, V. *Phys. Chem. Chem. Phys.* **2001**, *3*, 2735.
(51) Hirsch, M.; Quapp, W.; Heidrich, D. *Phys. Chem. Chem. Phys.* **1999**, *1*, 5291.

(52) Taketsugu, T.; Yanaia, T.; Hirao, K.; Gordon, M. S. *J. Mol. Struct. (THEOCHEM)* **1998**, *451*, 163.
(53) Quapp, W.; Heidrieh, D. *Theor. Chim. Acta* **1984**, *66*, 245.
(54) Kliesch, W. *J. Math. Chem.* **2000**, *28*, 91.
(55) Kliesch, W. *J. Math. Chem.* **2000**, *28*, 113.
(56) Quapp, W. *J. Mol. Struct.* **2004**, *695*−*696*, 95.
(57) Gonzalez-Lafont, A.; Moreno, M.; Lluch, J. M. *J. Am. Chem. Soc.* **2004**, *126*, 13089.
(58) Lasorne, B.; Dive, G.; Lauvergnat, D.; Desouter-Lecomte, M. *J. Chem. Phys.* **2003**, *118*, 5831.
(59) Leach, A. G.; Houk, K. N. *Chem. Commun.* **2002**, 1243.
(60) Castaño, O.; Palmeiro, R.; Frutos, L. M.; Luisandrés, J. *J. Comput. Chem.* **2002**, *23*, 732.
(61) Singleton, D. A.; Hang, C.; Szymanski, M. J.; Greenwald, E. E. *J. Am. Chem. Soc.* **2003**, *125*, 1176.
(62) Lee, T. J.; Taylor, P. R. *Int. J. Quantum Chem. Symp.* **1989**, *23*, 199.
(63) Noodleman, L. *J. Chem. Phys.* **1981**, *74*, 5737.
(64) Noodleman, L.; Davidson, E. R. *Chem. Phys.* **1986**, *109*, 131.
(65) Miller, C. E.; Francisco, J. S. *J. Phys. Chem. A* **2001**, *105*, 1662.

JP900484S